Testing the specificity of pharmacological tools in the study of calcium-activated chloride channels

Candidate number: VTDN3

Supervisor: Dr Martin Stocker

Figures: 14

Pages: 37

Words: 7471

Abstract

ANO1/TMEM16A and ANO2/TMEM16B are calcium (Ca^{2+})-activated chloride channels (CaCCs) and mediate important functions including fluid secretion, smooth muscle excitability and sensory signal transduction. Given their high Ca^{2+} sensitivity, it is likely that CaCCs contribute to modulating neuronal firing patterns in the central nervous system (CNS), working together with other ion channels, like Ca^{2+}-activated potassium channels (K_{Ca}). The dissection of the functional role of CaCCs in non-neuronal tissues have mainly relied on pharmacological testing. Previous high-throughput screening experiments have identified selective and potent TMEM16A-targeted compounds, including the inhibitor Ani9 (Adapted from Seo et al., 2016) and the activator E_{act} (Namkung et al., 2011). Because there are other Ca^{2+}-activated channels in the CNS, cross-reactivity of Ani9 and E_{act} with other expressing channels may be possible, causing misinterpretation of the CaCC roles in neurones. Aiming to investigate whether Ani9 and E_{act} may act on K_{Ca}-small conductance (SK)2 channels, whole-cell patch-clamp recordings on HEK293 cells expressing rSK2 were conducted in this study. The results show that neither Ani9 nor E_{act} appear to affect K_{Ca}-SK2 mediated currents, suggesting that these compounds are unlikely to cross-react with K_{Ca}-SK channels and may be promising pharmacological tools for studying the roles of CaCC in the CNS.

Declaration of contribution

Dr Stocker helped with cell culture preparation and Prof Pedarzani supervised me with the patch-clamp experiments. All experiments including data analysis are mainly by my own work. Any other data obtained from external work are explicitly referenced in the text.

Table of Contents

1. Introduction

The movement of chloride is tightly regulated in cells and mediated by different chloride channels and transporters, including Ca^{2+}-activated chloride channels (CaCCs), which are widely expressed in various organisms ranging from algae to neurones (Reviewed in Berg et al., 2012). These channels are activated by an increase in cytosolic Ca^{2+} in the 0.3-1.0 μM range (Scudieri et al., 2012) and contribute to different physiological processes, including fluid secretion, smooth muscle excitability and sensory signal transduction (Huang et al., 2012a). Although the existence of CaCCs was documented in frog oocytes in the 1980s (Cross, 1981), their molecular identity remained elusive until 2008, when three independent research groups (Caputo et al., 2008, Schroeder et al., 2008, Yang et al., 2008) identified ANO1 and ANO2 genes - encoding for anoctamin 1 and anoctamin 2 proteins (also referred as TMEM16A and TMEM16B in Xenopus) - as potential CaCC candidates.

Anoctamins belong to a family of proteins with striking functional diversity (Hartzell et al., 2009). In mammals, 10 members of anoctamins have been identified, named Ano1 through Ano10 (TMEM16A-H, TMEM16J and K, respectively). ANO1/TMEM16A and ANO2/TMEM16B are CaCCs, whereas all other TMEM16 paralogs, bar TMEM16H, are Ca^{2+}-dependent phospholipid scramblases. These scramblases are lipid transporters that facilitate the bidirectional diffusion of lipids between the inner and outer leaflet of the plasma membrane in an ATP-dependent manner, a process that is essential for the membrane biogenesis involved in physiological processes such as apoptosis (Suzuki et al., 2013). Unlike other scramblases which are non-ion selective, the mammalian TMEM16E (Boccaccio et al., 2019) and TMEM16F (Yu et al., 2015) show both ion

channel and lipid scramble activities. In fact, point mutations in the subunit cavity of TMEM16A are capable of converting the chloride channel into a scramblase and vice versa, highlighting the close relationship of the TMEM16 members (Le et al., 2019b). The founding members, TMEM16A and TMEM16B, exhibit hallmark properties of endogenous CaCCs, such that they activated by submicro- or micro-molar intracellular Ca^{2+} concentrations ($[Ca^{2+}]_i$). The currents they mediate are outwardly rectifying at low levels of $[Ca^{2+}]_i$, but become voltage-dependent at higher $[Ca^{2+}]_i$, showing a linear current voltage (I-V) relationship (Huang et al., 2012a) (Fig. 1A). TMEM16A and TMEM16B differ in some biophysical properties. For instance, besides TMEM16B being less sensitive to Ca^{2+} than TMEM16A (EC_{50} = 3-5 μM and EC_{50} = 0.4 μM respectively at +100 mV) (Xiao et al., 2011)), it also shows faster activation and deactivation kinetics (Fig. 1B) (Pifferi et al., 2009). Additionally, TMEM16B is found in different tissues to TMEM16A, predominantly in the retina, olfactory epithelia, and different neurones in the brain; whereas TMEM16A is primarily expressed in epithelial cells, smooth muscle cells and sensory neurones (Reviewed in Scudieri et al., 2012).

Previous studies used biochemical techniques such as chemical crosslinking to reveal that TMEM16A channels are assembled as homodimers (Sheridan et al., 2011, Fallah et al., 2011) (Fig. 2). More recent investigation using single-particle electron cryo-microscopy has further disclosed the mouse (m)TMEM16A structure at a higher resolution (Fig. 2B) (Paulino et al., 2017b, Dang et al., 2017), defining the structural basis for ion permeation and gating in TMEM16A. Together, these studies showed that each monomer contains 10-transmembrane (TM) α-helices with intracellular N- and C-terminal domains, contrary to the 8 previously predicted by hydropathy

analysis (Yang et al., 2008). Each subunit has its own pore formed by the TM3-8 α-helices, which is independently activated by the binding of two Ca^{2+} ions (Lim et al., 2016). TM3-7 forms the hourglass-shaped permeation pathway important for anion selectivity (Fig. 2C) (Dang et al., 2017, Paulino et al., 2017a) and T1, 2, 9 and 10 form the supporting dimer interface domain (Le et al., 2019a).

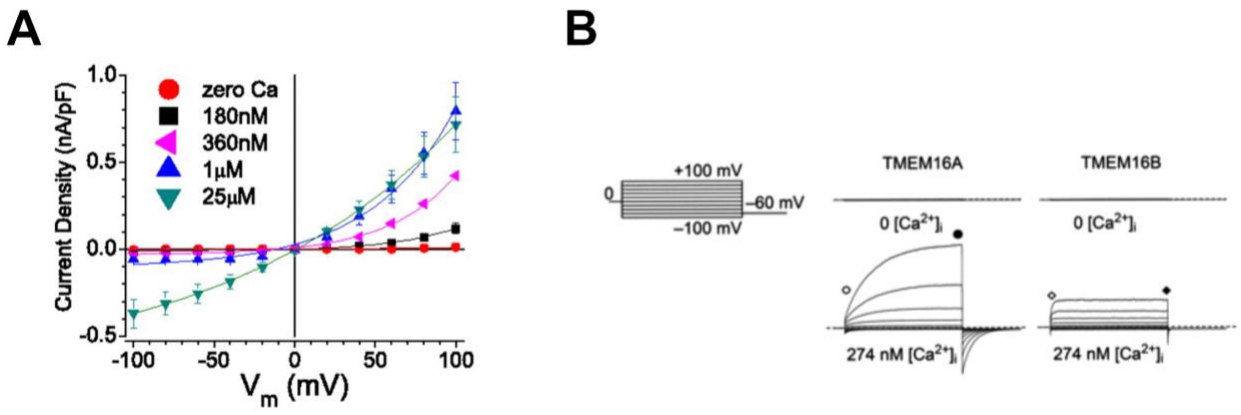

Figure 1 Biophysical properties of TMEM16A and TMEM16B. A) I-V relationship of TMEM16A showing the outward rectification at low $[Ca^{2+}]_i$ and voltage-dependent activation at high $[Ca^{2+}]_i$. (Taken from Xiao et al., 2011) **B)** Representative figure of whole-cell TMEM16A or TMEM16B currents in the presence of 0 or 274 nA $[Ca2+]_i$, showing that TMEM16B conducts less current than TMEM16A at the same level of $[Ca^{2+}]_i$ and displays faster activation and deactivation kinetics. (Adapted from Adomaviciene et al., 2013)

Previous studies have hypothesised the possible interaction between TMEM16A and calmodulin. However, electrophysiological testing on purified (h)TMEM16a proteins in liposomes showed that alone they are sufficient to form functional channels without the need for other proteins like calmodulin (Terashima et al., 2013). Indeed, site-directed mutagenesis experiments (Tien et al., 2014, Yu et al., 2014) have shown that the Ca^{2+}-binding site resides in the vicinity of the pore.

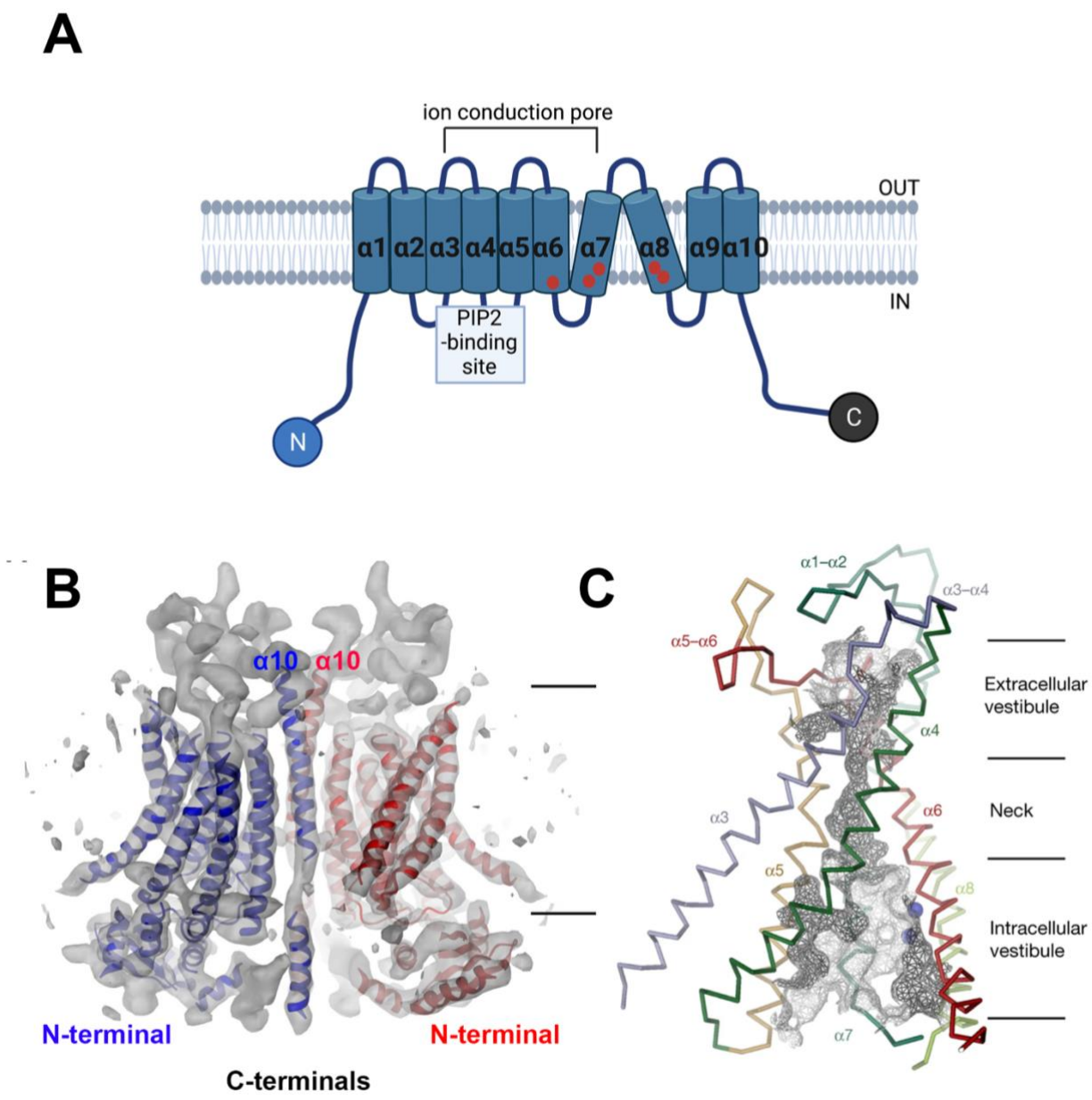

Figure 2 TMEM16A structure. A) A simplified topology of the TMEM16A monomer showing the 10-transmembrane α-helices, PIP-binding site (TM3-5), ion conduction pore (TM3-7), and the Ca^{2+}-binding site formed by the five acidic residues shown as red circles (TM6-8). **B)** Ribbon representation showing the electron microscopy (EM) density map of the mTMEM16A dimer. (Adapted from Paulino et al., 2017b) **C)** EM picture showing the hourglass-shaped ion conduction pore of the mTMEM16A subunit. (Taken from Paulino et al., 2017a)

Molecular reconstruction of TMEM16A with Cryo-EM indicated that the Ca^{2+}-binding site is located at the TM6-8 region made up of five highly conserved acidic residues E650, E698, E701, E730 and D734 (Fig. 2A) (Dang et al., 2017, Tien et al., 2014). The binding of Ca^{2+} to this site induces a conformational change of TM6, which releases the electrostatic gate imposed by the Ca^{2+}-binding acidic residues to directly induce pore opening (Lam and Dutzler, 2018, Dang et al., 2017, Paulino et al., 2017a). Interestingly, a recent study has identified a third Ca^{2+} binding site between TM2 and TM10, where Ca^{2+} binding enhances channel activation, revealing a potential mechanism of allosteric gating of TMEM16A channels (Le and Yang, 2020). During prolonged Ca^{2+}-dependent activation, TMEM16A channel desensitises. Inside-out patch-clamp recordings showed that PIP2 attenuates the desensitisation of TMEM16A under high Ca^{2+} levels, potentially by binding to a PIP2-binding site located at the cytosolic interface of TM 3-5 (Fig. 2A) (Le et al., 2019a). Thus, the rundown of CaCC in saturating Ca^{2+} may be explained by the regulatory effect of PIP2. Combined with electrophysiological studies, these experiments suggest that TMEM16A has multiple conformation states; binding of Ca^{2+} ions to one subunit is sufficient to open the channel at depolarised membrane potentials, while full occupancy of Ca^{2+} binding sites allows channel activation in a voltage-independent manner (Fig. 3) (Peters et al., 2018).

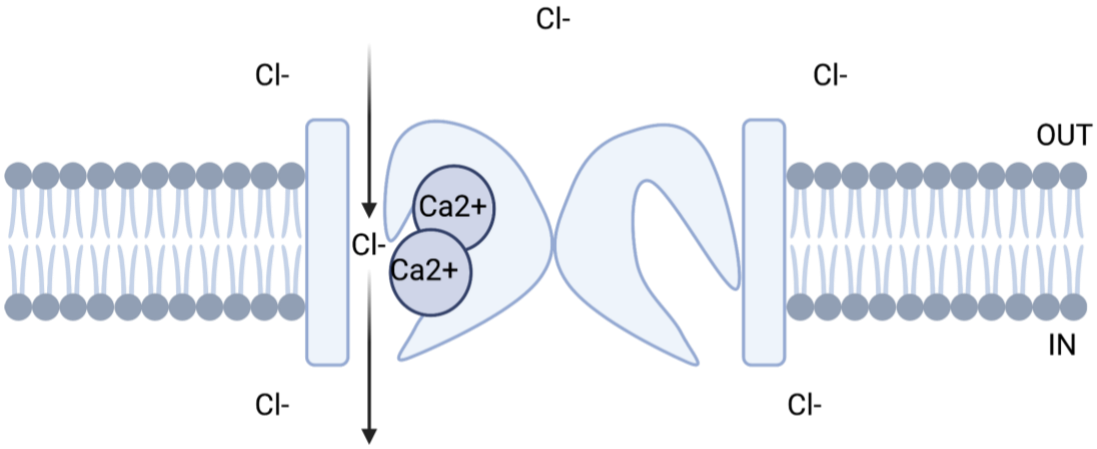

Figure 3 A simplified schematic illustrating a conceptual model of the TMEM16A gating mechanism. Binding of Ca^{2+} ions to a TMEM16A monomer is sufficient to induce channel opening in depolarised membrane potentials.

Ca^{2+}-activated potassium channels (K_{Ca}), like CaCCs, are also activated by an increase in $[Ca^{2+}]_i$ in nano- to micro-molar range. Activation of K_{Ca} channels causes membrane hyperpolarisation, an intrinsic feature that allows K_{Ca} channels to play a key role in regulating spike firing patterns and signal encoding in a concerted action with other ion channels (Pedarzani and Stocker, 2008). K_{Ca} channels are divided into three main members in accordance with their single channel conductance: SK (small conductance; 4-14 pS), IK (intermediate conductance; 32-39 pS) and BK (big conductance; 200-300 pS). SK channels are widely expressed throughout

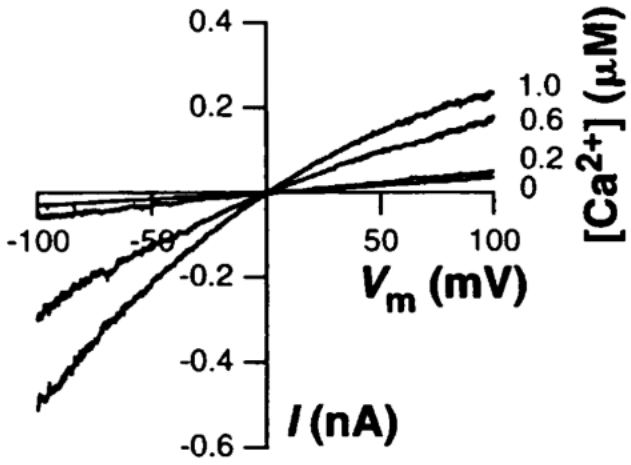

Figure 4 Biophysical properties of SK channels. Representative current traces showing the IV relationship of SK2 channels expressed in oocytes. Currents are intracellular calcium concentration-dependent, voltage-independent and display inward rectification. (Taken from Köhler et al., 1996)

the CNS, and three members of SK family (SK1, SK2 and SK3) have been cloned (Stocker and Pedarzani, 2000). These channels are activated by sub-micromolar $[Ca^{2+}]_i$ (EC_{50} = 0.3-0.7 μM) in a voltage-independent manner (Hirschberg et al., 1998) via the associated intrinsic Ca^{2+}-binding protein calmodulin (CaM) (Adelman, 2016). Calmodulin acts as a Ca^{2+}-sensor. Binding of Ca^{2+} to CaM forms the Ca-CaM complex, which in turn interacts with the calmodulin binding-domain (CaMBD) located in the proximal C-terminal of the channel to permit rapid channel gating. Although SK channels are voltage-insensitive, both native and cloned SK channels exhibit pronounced inward rectification when conducting outward current, hence showing a non-linear IV relationship (Fig. 4) (Köhler et al., 1996). This is due to a voltage-dependent block by intracellular divalent cations such as calcium itself (Soh and Park, 2001).

Given the high Ca^{2+} sensitivity of CaCCs and their presence in the CNS, CaCCs are also likely to contribute to an activity-dependent modulation of firing patterns and signal encoding in central neurones, activated in parallel to SK and other K_{Ca} channels. However, research in understanding the contribution of CaCC in neuronal firing is limited, mainly due to the delays in the molecular identification and a poor pharmacological profile (Verkman and Galietta, 2009). Having established the molecular identity of CaCCs, it would be interesting to explore the presence of CaCC currents mediated by TMEM16A and TMEM16B in the regulation of the firing activity of different neurones.

Pharmacological tools would be helpful for understanding the functional properties of CaCCs in neurones. Traditional drugs including niflumic acid (NFA) and 4,4′-diisothiocyano-2,2′-stilbenedisulfonic acid (DIDS) are often used as selective-CaCC inhibitors, but these lack

specificity because they may affect other chloride channels. For instance, NFA has been shown to cause emptying of Ca^{2+} stores in rat pulmonary artery smooth muscle cells which indirectly inhibits CaCCs (Cruickshank et al., 2003). Novel putative TMEM16A and TMEM16B-selective drugs have been identified through high-throughput screening of a large chemical library, including activators like naroylaminothiazole (Eact) (Namkung et al., 2011), as well as inhibitors such as CaCCinh-A01, T16Ainh-A01, MONNA, etc. (Seo et al., 2016). To date, the TMEM16A inhibitor 2-(4-chloro-2-methylphenoxy)-N-[(2-methoxyphenyl)methylideneamino]-acetamide (Ani9) has been shown to be the most potent and selective human ANO1/TMEM16A inhibitor, with an IC_{50} of less than 3 μM (Seo et al., 2016). Conversely, E_{act} can activate TMEM16A (EC_{50} = 3-6 μM) and TMEM16B to a lesser extent (EC_{50} not known) (Namkung et al., 2011). The potential selectivity of Ani9 and E_{act} suggests that their potential application for dissecting TMEM16A and TMEM16B function in the CNS. However, the selectivity of these drugs to other channels, particularly Ca^{2+}-activated channels like $K_{Ca,}$ is unknown. This could be problematic, as a cross-reactivity of TMEM16A and TMEM16B CaCC-inhibitors and activators with K_{Ca} channels may be possible, which can lead to misinterpretation of the CaCC roles in neurones. In this study, the effect of TMEM16A and TMEM16B inhibitor Ani9 and activator E_{act} on SK2-mediated currents (I_{SK2}) is measured using the whole-cell patch-clamp technique to test the specificity of these drugs for the study of CaCC.

2. Methods

2.1. Materials and Solutions

E_{act} and Ani9 were obtained from Tocris Bioscience (Bristol, UK) and were dissolved in dimethyl sulfoxide (DMSO) stock solution. Solutions needed for cell culture including the selection marker geneticin G418, phosphate buffered saline (PBS), L-glutamine, 0.05% Trypsin/0.02% EDTA and DulbeccoMEM (DMEM) were all from Gibco-BRL (Paisley, UK). All other salts and chemicals, including Tetraethylammonium (TEA), were obtained from either Merck or Sigma-Aldrich (Dorset, UK).

2.2. Cell culture

HEK293 cell line heterologously expressing rSK2 channels was generated in the host lab (University College London, London, UK). Cells were grown in cell culture flask (T25) with 5 mL DMEM/F12 medium, supplemented with L-glutamine (2 mM), 10% FCS, Penicillin (100 U/ml)/Streptomycin 100 µ/ml/ and geneticin (G418, 400 µg/ml) for selection. Upon reaching ~90% confluency, cells were rinsed with PBS, trypsinised (2-3 minutes) and split at a ratio of 1:10. To prepare for electrophysiological recordings, cells were trypsinised, and plated onto poly-D-lysine-coated glass coverslips in 1 ml complete DMEM/F12 medium without G418 and incubated overnight. Cells were kept in a humidified incubator (5% CO_2) at 37°C.

2.3. Electrophysiological recordings

Whole-cell patch-clamp recordings were made at room temperature (22°C) on HEK293 cells expressing rSK2 channels. Data were acquired using an EPC10 amplifier (HEKA, Lambrecht, Germany) controlled by the programme Pulse (v8.8) software (HEKA, Lambrecht, Germany). Data were filtered at 5 kHz and digitised at 20 kHz.

The pipette intracellular solution contained 115 mM KGluconate, 10 mM KCl, 10 mM HEPES and 10 mM EGTA (pH 7.21 with KOH, 300 mOsm/kg H_2O), with a free metal concentration of 1 mM Mg^{2+} and 1 µM free Ca^{2+} (adding 1.06 mM $MgCl_2$ and 8.75 mM $CaCl_2$) based on calculations made with the programme MaxChelator (Webmaxc Extended, Stanford, USA). Pipettes were pulled from borosilicate glass with a vertical patch electrode puller, and pipettes' resistances ranged from 3 to 10 megaohms when filled with intracellular solution. Seal resistances were between 1 to 3 gigaohms. Upon forming gigaseal, the fast capacitative transients were automatically compensated.

Cells were perfused at a flow rate of 1-2 mL/min with either a physiological [K^+] ringer or symmetrical [K^+] ringer. Cells were patched at physiological/low extracellular [K^+] ($[K^+]_{low}$) (inside K^+ concentration ($[K^+]_{in}$) = 115mM; outside K^+ concentration ($[K^+]_{out}$) = 4mM) which contained 4 mM KCl, 140 mM NaCl, 2 mM $CaCl_2$ and 1 mM $MgCl_2$, 10 mM HEPES and 10 mM D-glucose (pH 7.4 with NaOH, 305-310 mOsm H_2O). Recordings were performed in symmetrical/high extracellular K^+ ($[K^+]_{high}$) conditions ($[K^+]_{in}$ = 115mM; $[K^+]_{out}$ = 144mM) which contained 144 mM KCl, 2 mM $CaCl_2$ and 1 mM $MgCl_2$, 10 mM HEPES and 10 mM D-glucose (pH 7.4 with KOH, 305-310 mOsm/kg

H_2O). Whole-cell currents were recorded by ramping the voltage from -140 mV to +60 mV for 400 ms, at a holding potential of 0 mV in symmetrical [K^+] ringer. Stock solutions of inhibitor Ani9 (10 mM) and small organic activator E_{act} (50 mM) were prepared in 100% DMSO. Compounds were diluted in symmetrical [K^+] ringer to be applied to the cells for 3 minutes. Leak currents were verified upon suppression of the TEA-sensitive I_{SK2} by 100 mM TEA either in the beginning and the end of every recording, or only at the end. In the TEA-containing solution, 100 mM TEA-Cl replaced the 100 mM KCl in the symmetrical [K^+] ringer. Cells that showed more than 10% residual current after application of 100 mM were excluded from the analysis.

2.4. Data and statistical analysis

Voltage-clamp data were analysed with IGOR (v6.12, Wavemetrics, Oregon, USA). The whole-cell currents were analysed at -40 mV as measurements at more negative voltages were saturating for some experiments. Data were then tabulated and statistically analysed using GraphPad Prism software (v9.3.1, Graphpad Software Inc., San Diego, CA, USA). Two tailed Student's paired t-test was used for statistical comparisons of the current amplitudes measured in drug and without drug. One-sample t-test was used to analyse relative effect of I_{SK2} by the drug. Values are reported as relative current left (%) or means ± S.E.M, depending on the statistical method used. The difference between data sets was considered significant when $P < 0.05$.

3. Results

3.1. Effects of the inhibitor Ani9 on TMEM16A- and TMEM16B-mediated Calcium-activated Chloride currents in HEK293 cells

Whole-cell patch-clamp experiments were performed to study the effect of Ani9 on TMEM16A ($I_{TMEM16A}$) and TMEM16B currents ($I_{TMEM16B}$) in HEK293A cells expressing human (h) hTMEM16A or mouse (m) mTMEM16B (unpublished data kindly provided by Dr. Boccaccio, Institute of Biophysics, Consiglio Nazionale delle Richerche, Genova, Italy). Cells were held at 0 mV in a solution with near-symmetrical chloride concentrations (inside Cl- concentration = 130 mM and outside Cl- concentration = 140 mM). TMEM16A or TMEM16B-mediated currents were elicited by voltage steps from -60 to +140 mV, in the presence of 260 nM intracellular free Ca^{2+}. Voltage was stepped in 20 mV increments for 500 ms for TMEM16A and 300 ms for TMEM16B, before stepping back to -80 mV for tail current analysis.

As expected, $I_{TMEM16A}$ and $I_{TMEM16B}$ recorded in HEK293A cells possessed TMEM16A and TMEM16B channel kinetics. At high voltage steps, TMEM16A currents did not reach steady state but continues to slowly increase or decrease at increasing pulse duration, showing that TMEM16A currents are time-dependent and possess slow activation and deactivation kinetics upon depolarisation or repolarization (Fig. 5A). In contrast, $I_{TMEM16B}$ does appear to reach steady state, indicating fast activating and deactivating kinetics, as illustrated by the more rapid declining tail currents compared to those of TMEM16A (Fig. 6A). The activation of both $I_{TMEM16A}$ and $I_{TMEM16B}$ follow a mono-exponential time-course and are outwardly rectifying, as indicated by the

decreasing current amplitudes at negative voltages but increasing amplitudes at depolarised voltages (Fig. 5A and 6A). However, the outward rectification is less pronounced in $I_{TMEM16B}$ (Fig. 6A).

3 μM Ani9 significantly reduced the current amplitudes evoked at the test potentials range and prolonged their activation and deactivation kinetics, eliminating the mono-exponentiality. This current was completely abolished by 30 μM Ani9 (Fig. 5B and C). Conversely, application of Ani9 (30μM) did not show a prominent reduction in $I_{TMEM16B}$ amplitudes, and only a partial inhibition (~37%) with high Ani9 concentration (300 μM) (Fig. 6A and B). The observed currents showed a reversal potential close to 0 mV for both TMEM16A and TMEM16B which corresponds to the potentials predicted by the Nernst equation for a chloride conductance (V_m = 1.96 mV).

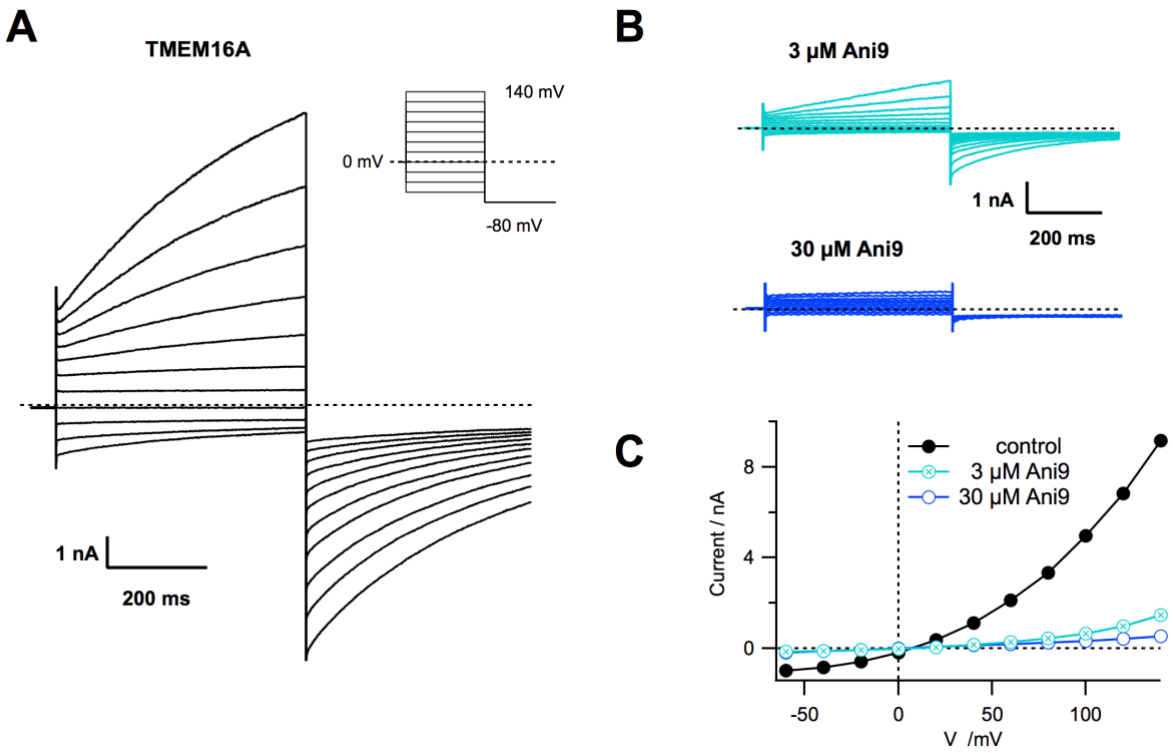

Figure 5 A and B) Representative current traces of TMEM16A - obtained using the protocol illustrated in the inset of **(A)** - without **(A)** and with **(B)** Ani9 application of 3 µM (light blue traces) and 30 µM (dark blue traces) concentrations. **C)** I-V relationship of TMEM16A currents without (black circles) and with 3 µM (light blue crossed circles) or 30µM (dark blue circles) Ani9. (Unpublished data by Dr. Boccaccio)

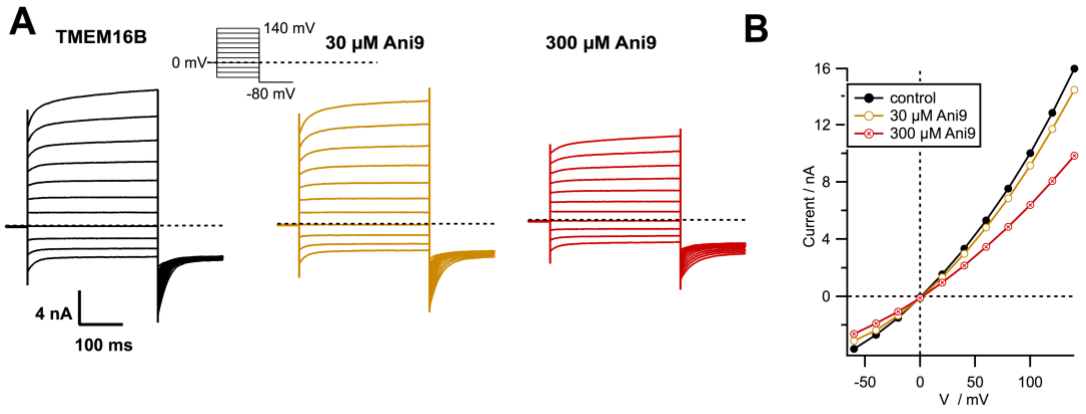

Figure 6 A) Representative current traces of TMEM16B, obtained using the protocol illustrated in the inset on the (left), in the presence of 30 µM (centre) and 300 µM (right) Ani9. **B)** I-V relationship of TMEM16B currents without (black circles) and with 30 µM (yellow circles) or 300 µM (red crossed circles) Ani9. (Unpublished data by Dr. Boccaccio)

3.2. The modulatory effect of Eact on TMEM16A and TMEM16B-mediated Calcium-activated Chloride currents

The modulatory effect of E_{act} has been shown by whole-cell patch-clamp recordings in HEK293 cells overexpressing human (h)TMEM16A (Centeio et al., 2020). Membrane voltages were clamped in steps of 20 mV from -100 mV to 100 mV, from a holding potential of -100 mV and with basal $[Ca^{2+}]_i$ (0.1 µM). E_{act} potently activated TMEM16A channels (EC_{50} = 3 µM) as shown by the clear increase in the amplitude of the current traces with E_{act} compared to controls (Fig. 7A). E_{act} also clearly enhanced the outward rectification of $I_{TMEM16A}$, as illustrated in Fig. 7B. Moreover, the $I_{TMEM16A}$ amplitude increased by approximately 10-fold at depolarised potentials (100 mV) in the presence of E_{act} compared to controls (Centeio et al., 2020), indicating that E_{act} acts as a potentiator of $I_{TMEM16A}$ (Fig. 7B).

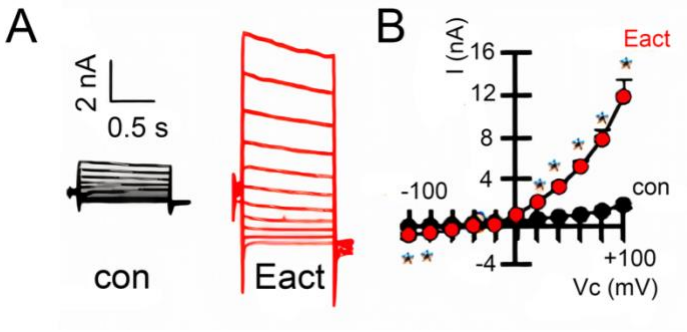

Figure 7 Patch-clamp analysis showing the response of overexpressed TMEM16A to E_{act}. **A)** Representative current traces induced by voltage steps from -100 mV to 100 mV, control TMEM16A currents (black) and TMEM16A currents potentiated by E_{act} (red). **B)** Summary of I-V relation (graph on the right) of control (black) TMEM16A currents and with E_{act} (red). (Adapted from Centeio et al., 2020)

Besides TMEM16A, E_{act} has also been reported to activate $I_{TMEM16B}$ in Fischer Rat Thyroid (FRT) cells transfected with mTMEM16B. Whole-cell currents were elicited by applying hyperpolarising

and depolarising voltage pulses in the range of -100 mV to 100 mV in steps of 20 mV, holding at 0 mV and in the absence of $[Ca^{2+}]_i$. E_{act} produced a substantial, concentration-dependent increase in $I_{TMEM16A}$ in mTMEM16A-transfected cells (Fig. 8). Likewise, E_{act} (10µM) also potentiated $I_{TMEM16B}$, however the current activation did not sustain but decreased after reaching its maximum amplitude (Namkung et al., 2011), suggesting that the effect of E_{act} on TMEM16B is less prominent compared to TMEM16A.

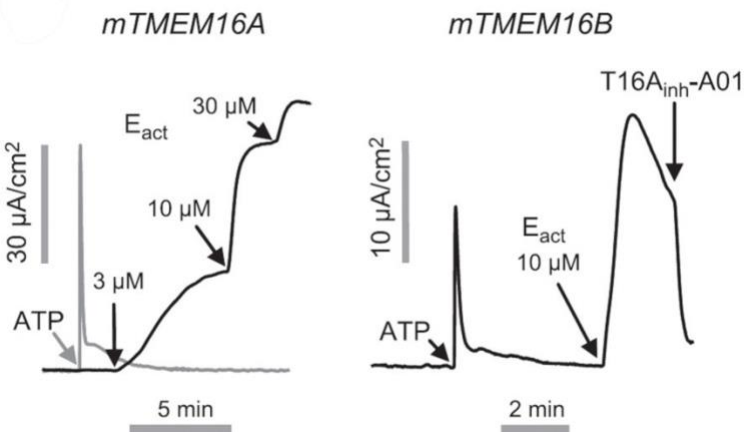

Figure 8 Patch-clamp currents measured in FRT cells transfected with mTMEM16A (left) and mTMEM16B (right). Different E_{act} concentrations (3, 10 and 30 µM) were applied on TMEM16A and 10 µM E_{act} was applied to TMEM16B. 100 µM ATP was applied as controls producing a large transient elevation in chloride current in both channels (shown as grey trace when applied to TMEM16A). T16Ainh-A01 was applied to block TMEM16B. (Taken from Namkung et al., 2011)

3.3. HEK293 cells transfected with rSK2-channels show characteristic potassium currents using the standard protocol

TMEM16A and TMEM16B inhibitor Ani9 and activator E_{act} could be useful for targeting CaCCs pharmacologically in neurones to dissect these channels' functions. To avoid possible misinterpretation of the CaCC roles, it is important to establish the specificity of these drugs and ensure that they do not act on other Ca^{2+}-activated channels, like K_{Ca}-SK2 channels. With a view

to testing whether Ani9 and E_{act} may affect I_{SK2}, the response of rSK2 channels to these drugs in HEK293 cells was recorded using the whole-cell patch-clamp technique with the following standard protocol.

Upon reaching whole-cell configuration at physiological [K^+] conditions, rSK2 channels were activated by 1 µM free Ca^{2+} in the patch pipette. Subsequent recordings of I_{SK2} were made in symmetrical [K^+] conditions to allow analysis of inward currents, thereby avoiding the variable rectification seen for outward I_{SK2} under physiological conditions (Nolting et al., 2007). The current was recorded by ramping the voltage from -140 to +60 mV over 400 ms, from a holding potential of 0 mV. The inward currents recorded at -40 mV ranged from 1.5 to 20 nA, with a mean amplitude of 8.6 ± 0.68 nA (n = 45). Before and after, or only after drug application, 100 mM TEA was applied to block I_{SK2}, ensuring that the observed current was predominantly due to SK-activation. A negligible non-SK channel dependent leak current was observed after TEA application. The reversal potential of I_{SK2} in symmetrical [K^+] ringer was close to the predicted values

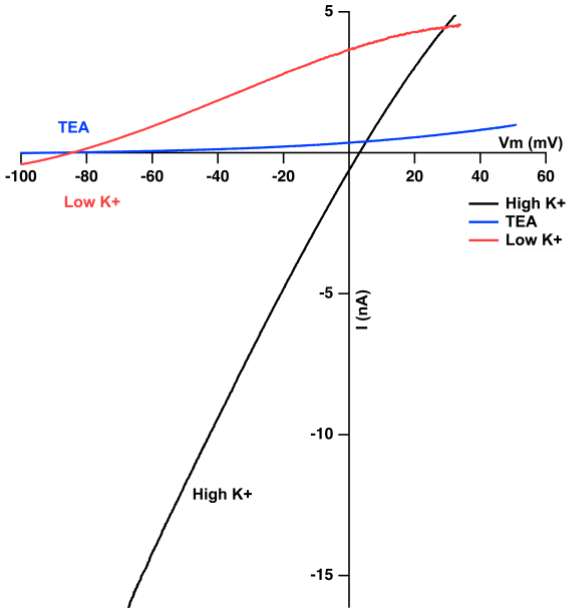

Figure 9 I-V plot from one of the representative experiments showing the TEA inhibition (red traces), and the shift in reversal potential of the SK2-mediated currents observed in symmetrical K^+ ($EK_{high} \approx 5.66$ mV) (black traces) and in physiological [K^+] conditions ($EK_{low} \approx -84.6$ mV) (red traces). Notice that TEA inhibition leaves a very small non-SK mediated residual current.

calculated using the Nernst equation (EK_{high} ≈ 5.66 mV). At the end of each experiment, the $[K^+]_{out}$ was lowered back to physiological conditions (4 mM), and the reversal potential of the observed currents would shift to hyperpolarising values (EK_{low} ≈ -84.6 mV) (Fig. 9).

3.4. DMSO does not affect the calcium-activated potassium currents elicited in HEK293 cells heterologously expressing rSK2 channels.

Dimethylsulfoxide (DMSO) is commonly used as solvent for many pharmacological compounds thanks to its amphiphilic and high polarity properties (Rodriguez-Buford et al., 2002). However, the molecular mechanisms associated with DMSO is unclear and studies have noticed unwanted effects by DMSO on cells like ovarian carcinoma cells (Rodriguez-Buford et al., 2002). In this study, the CaCC pharmacological compounds were dissolved in 100% DMSO. To avoid any potential misinterpretation of the results and to ensure that the observed effects of the application of Ani9 or E_{act} on I_{SK2} are not due to DMSO, the effect of DMSO alone was tested on rSK2 channels.

Two concentrations of DMSO (0.1% and 1%) were tested as these correspond to tested concentrations of Ani9 and E_{act}. During 3-minutes DMSO application in symmetrical [K+] at -40 mV, whole-cell I_{SK2} was stable for both concentrations (Fig. 10A and C). Further IV analysis showed that the I_{SK2} in the presence of 0.1% or 1% DMSO produced the same linear SK-mediated inward current as controls, both reversing at near the expected EK_{high}. Moreover, the I_{SK2} left rafter 0.1% or 1% DMSO application was not significantly different to controls (DMSO 0.1%: 92% ± 8, n=5; DMSO 1%: 98% ± 4.1, n=5; Fig. 10E and F). In contrast, 100 mM TEA completely inhibited the I_{SK2} (2.2% ± 1, n=5, $P < 0.0001$; Fig. 10B, D and G) within seconds of its application, and the

inhibition was fully reversible with washout (Fig. 10A and C), confirming that the observed currents were indeed SK-mediated. These results indicate that DMSO at these concentrations has no effect on SK2-channels expressed in HEK293 cells.

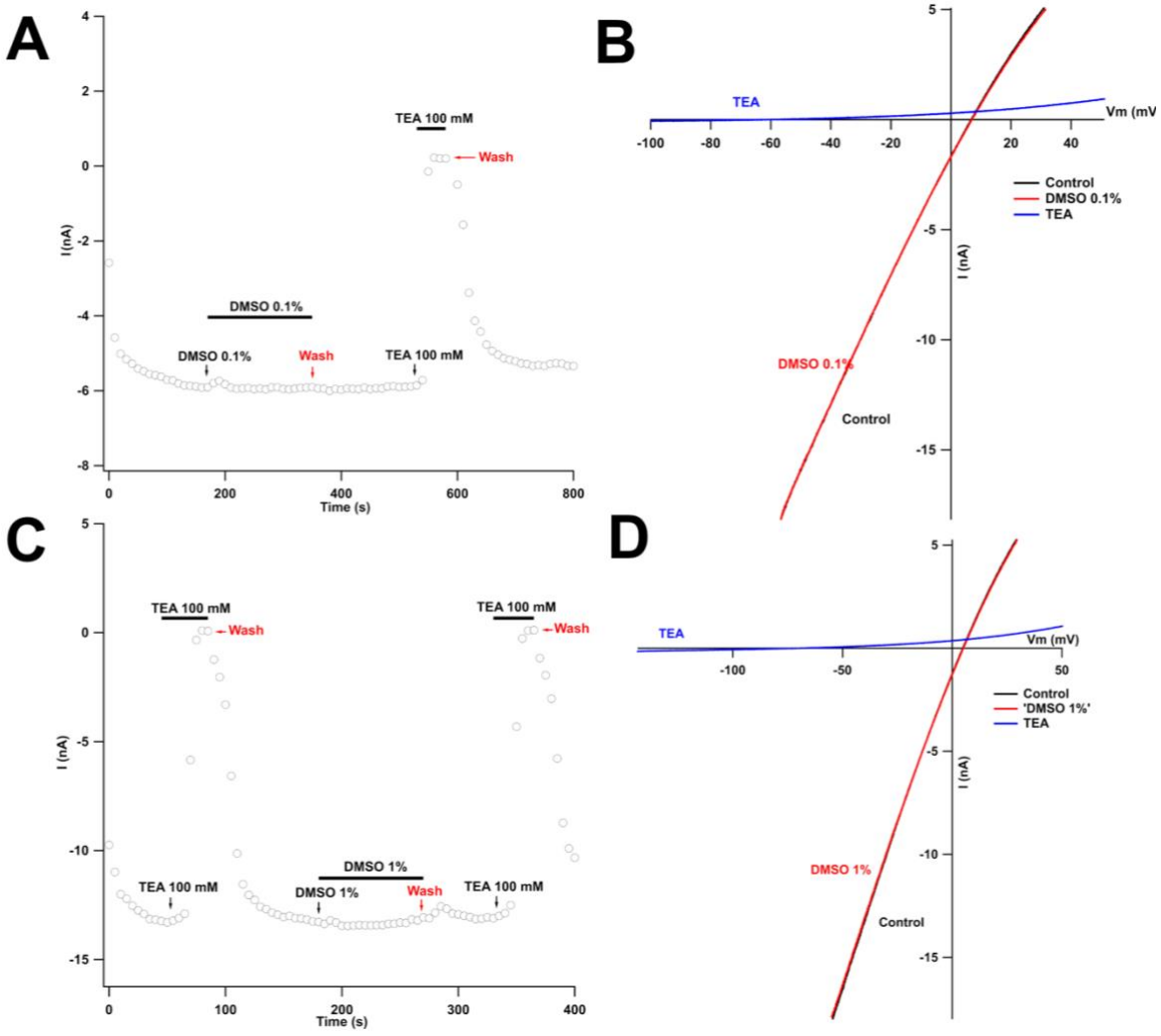

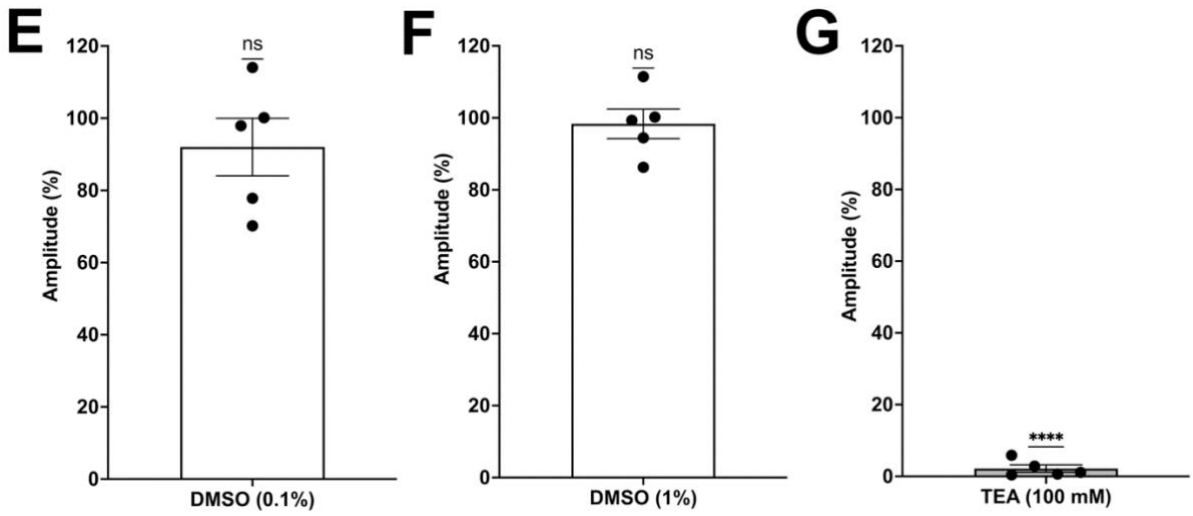

Figure 10 DMSO does not affect rSK2 currents. A and C) Representative time-courses of whole-cell I_{SK2} amplitudes at -40 mV upon drug application for 0.1% **(A)** and 1% DMSO **(C),** with the corresponding washouts and TEA application for controlling the stability of the recordings. TEA was applied after 0.1% DMSO was applied **(A),** and before and after 1% DMSO **(C). B and D)** The corresponding I-V plots of the experiment A and C comparing the last current traces taken during the application of 0.1% **(B)** and 1% DMSO **(D**) to those of control and application of 100 mM TEA. **E to G)** Summary diagrams comparing the relative (%) inhibition of I_{SK2} by 0.1% DMSO (92% ± 8, P> 0.05; **E**), 1% DMSO (98% ± 4.1, P> 0.05; **F**) and TEA (100 mM, 2.2% ± 1, P< 0.0001; **G**) on I_{SK2} recorded from 5 cells per group. Symbols represent individual experiments, bars are mean ± SEM.

3.5. The effect of Ani9 on rSK2 channels

Having established that DMSO does not affect the SK2-currents recorded in HEK293 cells, the effect of Ani9 on SK2-channels was subsequently investigated. As the IC_{50} of Ani9 has been established to be 3 μM and the CaCC currents were fully inhibited by Ani9 at 30 μM, these concentrations were selected to be used for testing on the rSK2.

To investigate whether Ani9 exerts any inhibitory effect on SK2-channels, whole-cell currents

activated by 1 µM Ca^{2+} were recorded. 3 µM or 30 µM Ani9 was applied for 3 minutes to an HEK293 cell expressing rSK2 in symmetrical [K^+], followed by a 3-minutes washout (Fig. 11A and C). Like before, the complete and reversible inhibition by 100 mM TEA before and after Ani9 application demonstrated the stability of the recording conditions throughout the drug application (Fig. 11A and C). Interestingly, right upon the application of both 3 µM and 30 µM Ani9, a transient partial reduction of I_{SK2} was observed in some cells (Fig. 11A and C). However, at the end of the Ani9 application, the current amplitudes stabilised at the same current amplitude observed before Ani9 application in all cells (Fig. 11A and C). Indeed, the IV curve of the last I_{SK2} trace with 3 µM or 30 µM applied is almost identical to that of control, both reversing at the same reversal potential close to EK_{high} (Fig. 11B and D). This fast transient inhibition is potentially a consequence of not using all lines of the perfusion system, allowing a small amount of TEA to remain in the dead space of the manifold (and empty lines). However, it is surprising that this was not also seen for the DMSO experiments, and alternative explanations might exist, which suggests further experiments are necessary to find out whether this is indeed due to perfusion system or a real effect of Ani9 on SK2 channels. Nonetheless, the current reduction by either 3 µM or 30 µM Ani9 (applied for three minutes) was negligible (3 µM: -0.071 ± 0.17 nA, n=7; 30 µM: -0.2 ± 0.25 nA, n=7; Fig. 11E, F), suggesting that Ani9 with concentrations of up to 30 µM does not inhibit I_{SK2} in HEK293 cells.

To ensure that the results are not affected by DMSO, the drug effects of 3 µM and 30 µM Ani9 were compared to their corresponding percentage of DMSO. Neither concentrations of Ani9 showed any statistical difference on drug effect compared to that of DMSO (6.5 ± 7.1%, P= 0.38; -2.3 ± 4.6%, P= 0.6214, respectively), indicating that DMSO did not contribute to the observed

effect of Ani9 on I_{SK2} in HEK293 cells (Fig. 12A and B).

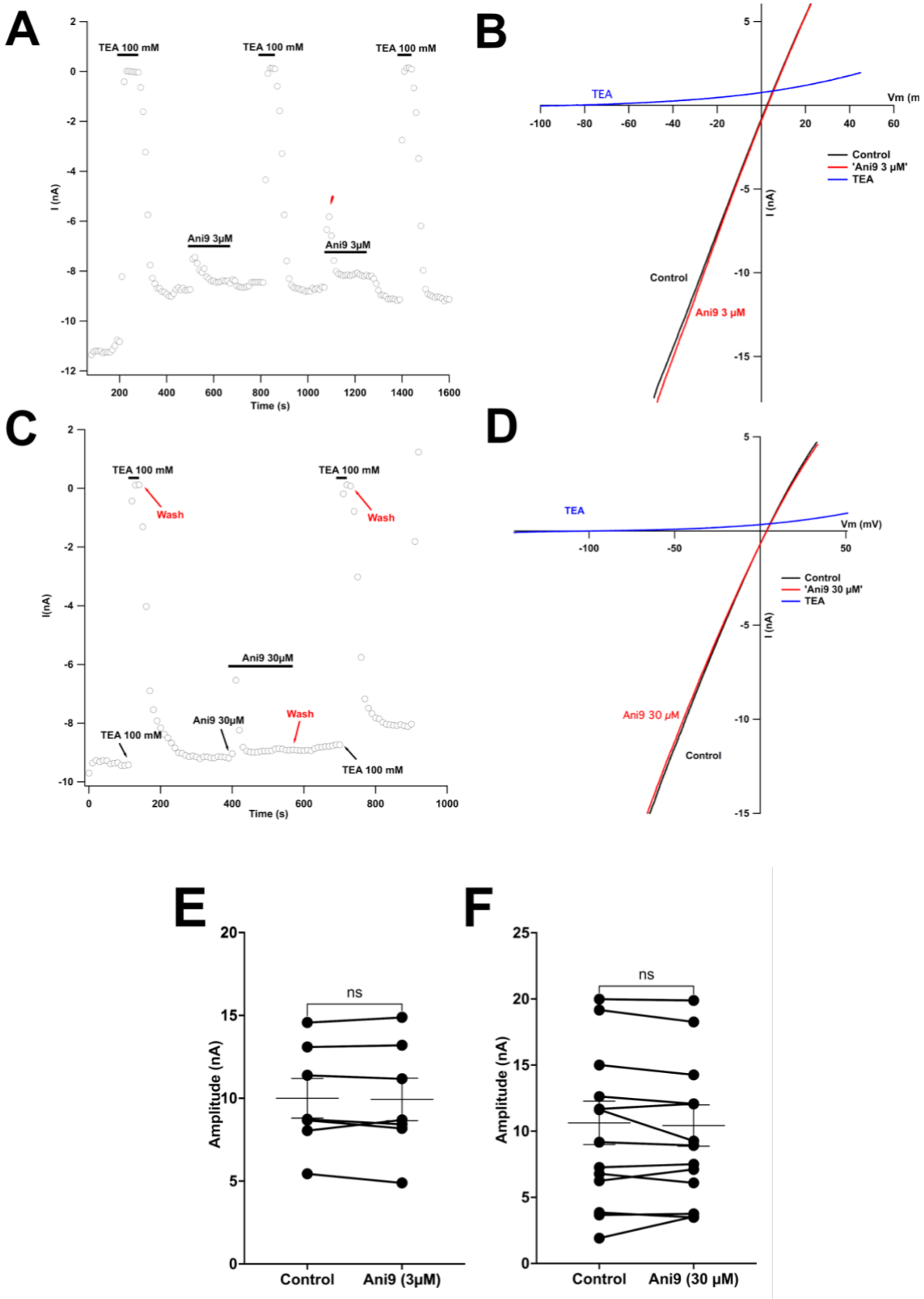

Figure 11 Ani9 does not exert inhibitory effect on rSK2 currents. A and C) Representative time courses of whole-cell I_{SK2} amplitudes at -40 mV upon application of drugs for 3 μM **(A)** and 30 μM **(C)**, the washout and the control for stability of the recording, the absent of leak current (100 mM TEA). The transient reduction of SK-current upon application of Ani9, which is discussed above, is indicated by a red arrow. **B and D)** The corresponding I-V plots of the experiment A and C comparing the last current traces taken during the application of 3 μM **(B)** and 30 μM Ani9 **(D)** to those of control. As expected, inhibition by TEA (100 mM) leaves only small non-SK mediated residual currents. **E and F)** Summary diagrams showing the difference in mean current amplitude between control and with application of 3 μM (-0.071 ± 0.17 nA, P> 0.05; **E)** or 30 μM Ani9 (-0.2 ± 0.25 nA, P> 0.05; **F)** on I_{SK2} recorded from 7 cells for each concentration. Symbols represent individual experiments, bars are mean ± SEM.

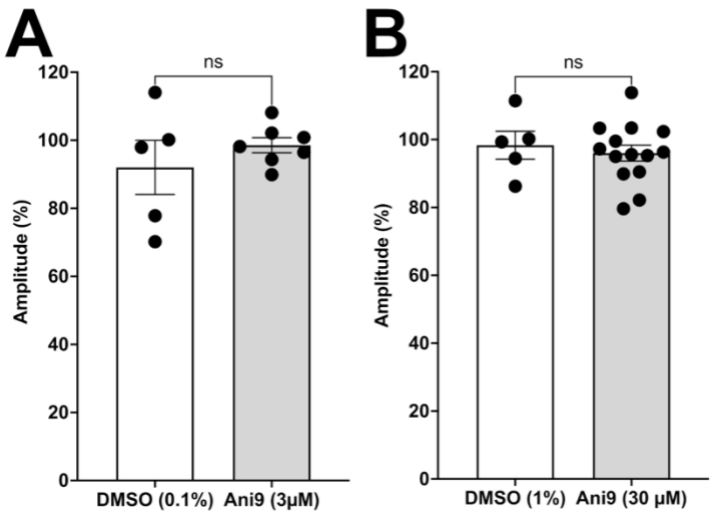

Figure 12 Bar diagrams comparing the relative effect of I_{SK2} by 0.1% DMSO to 3 μM Ani9 (6.5 ± 7.1%, P= 0.38; **A**)**,** and by 1% DMSO to 30 μM Ani9 (-2.3 ± 4.6%, P= 0.6214; **B**). Symbols represent individual experiments, bars are mean ± SEM.

3.6. The effect of Eact on rSK2 channels

The effect of the TMEM16A activator E_{act} on SK2 channels was also explored. 10 μM and 30 μM of E_{act} were selected to be examined using the same experimental protocol as previously described. Like Ani9, whole-cell inward I_{SK2} activated by 1 μM Ca^{2+} was not significantly affected by E_{act} at either concentration (Fig. 13A, C). Indeed, I_{SK2} responses to voltage ramps applied in symmetrical extracellular $[K^+]_{out}$ conditions in the presence of E_{act} at either concentration

overlapped with controls, as illustrated in the I-V plots (Fig. 13B and D). Application of 100 mM TEA once again fully blocked I_{SK2} confirming the stability of the recordings (Fig. 13A-D). The difference between the I_{SK2} in the presence of either 10 µM or 30 µM E_{act}, and the mean control amplitudes, was negligible (n=7; E_{act} 10 µM: -0.24 ± 0.15 nA; E_{act} 30 µM: 0.54 ± 0.44 nA; Fig. 13E and F), suggesting that E_{act} in concentrations of up to 30 µM does not potentiate nor inhibit I_{SK2} in HEK293 cells. Again, to confirm that the effect of E_{act} on I_{SK2} was not conditioned by DMSO, the relative drug effects of 10 µM and 30 µM E_{act} were compared to 0.1% (Fig. 14A) and 1% DMSO (Fig. 14B) and no significant difference was observed (3.4 ± 7.8%, P= 0.6714; -4.5 ± 5.8%, P= 0.4517, respectively), confirming the observed effects of E_{act} on I_{SK2} are reliable.

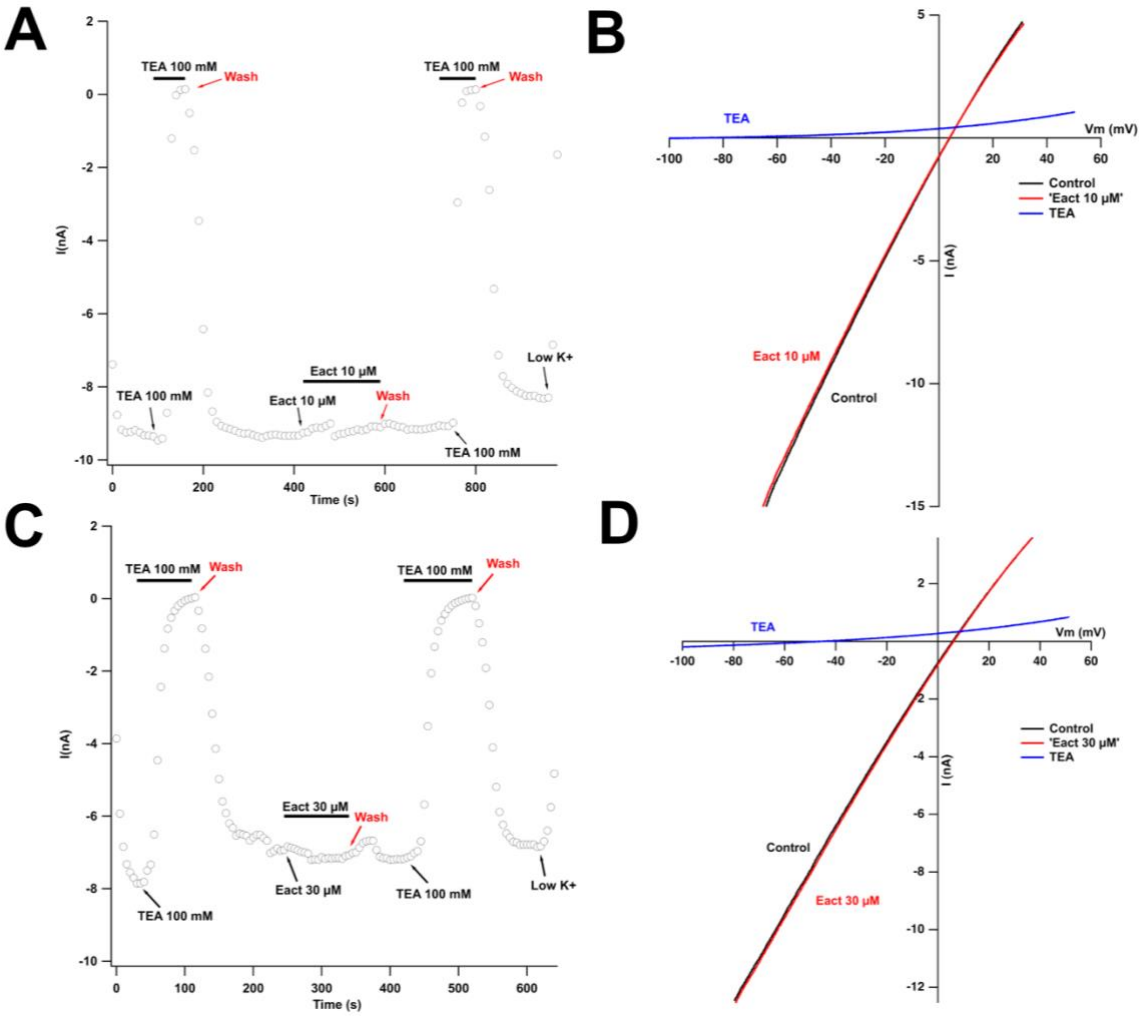

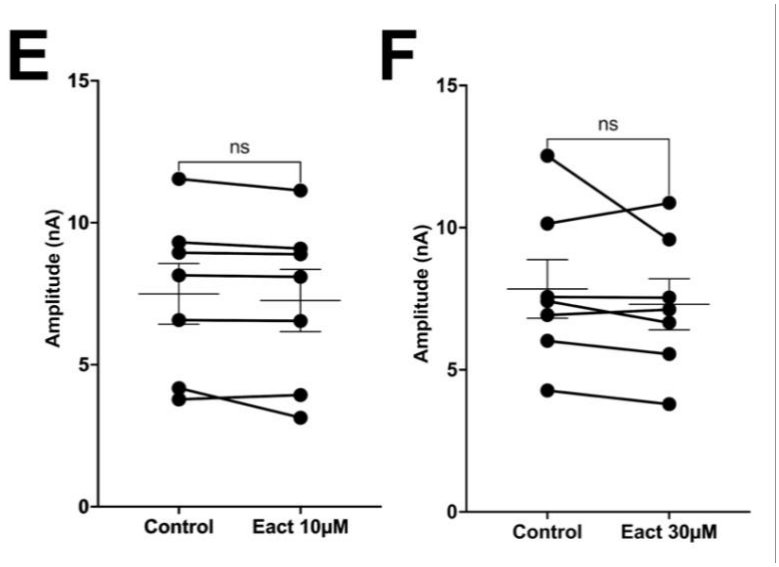

Figure 13 E_{act} does not affect rSK2 currents. A and C) Representative time courses of whole-cell current amplitudes at -40 mV upon application of drugs for 10 μM **(A)** and 30 μM **(C)** E_{act}, with the corresponding washouts and application of TEA for stability control of the recordings. **B and D)** The corresponding I-V plots of the experiment A and C comparing the last current traces taken during the application of 3 μM **(B)** and 30μM E_{act} **(D)** to those of control and of 100 mM TEA. **E and F)** Summary diagrams comparing the difference in mean current amplitude between control and with application of 10 μM (n=7, -0.24 ± 0.15 nA, P > 0.05; **E)** or 30 μM E_{act} (n=7, 0.54 ± 0.44 nA, P > 0.05; **F**) on I_{SK2} recorded from 7 cells for each concentration. Symbols represent individual experiments, bars are mean ± SEM.

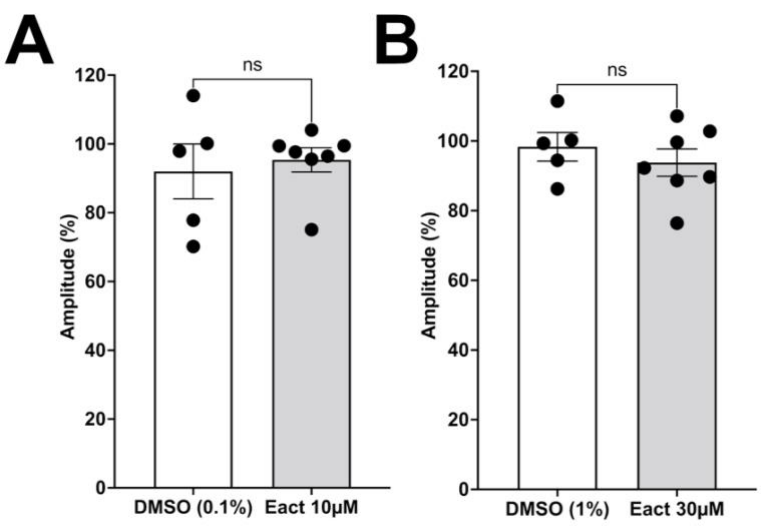

Figure 14 Bar diagrams comparing the relative effect of I_{SK2} by 0.1% DMSO to 10 μM E_{act} (3.4 ± 7.8%, P= 0.6714; **A**), and by 1% DMSO to 30 μM E_{act} (-4.5 ± 5.8%, P= 0.4517; **B**). Symbols represent individual experiments, bars are mean ± SEM.

4. Discussion

Different TMEM16A and TMEM16B-targeted compounds have been characterised but are surprisingly diverse in their structure, raising questions regarding their specificity (Kunzelmann et al., 2019). Given these channels' sensitivity to Ca^{2+}, the electrophysiological response of TMEM16A and TMEM16B with other Ca^{2+}-activated channels, such as K_{Ca}, may be similar and both types of channels might be activated simultaneously in the presence of Ca^{2+}. This means that pharmacological tools targeting TMEM16A and TMEM16B may cross-react with K_{Ca}. This study investigated the specificity of the TMEM16A and TMEM16B small molecule modulators Ani9 and E_{act} on K_{Ca}-SK2 channels. Whole-cell patch-clamp recordings showed that neither Ani9 nor E_{act}, in concentrations up to 30 μM, produced any significant effect on I_{SK2} in HEK293 cells, suggesting that they are unlikely to act on K_{Ca}-SK channels.

Options for TMEM16A and TMEM16B activators are currently limited. The most well-known one is E_{act}, which has been used in several studies to assess the role of TMEM16A activation in different physiological processes. It has been reported that E_{act} can stimulate both human epithelial chloride secretion and murine intestinal smooth muscle contraction (Namkung et al., 2011), as well as inhibit oestradiol production in cultured mouse granulosa cells (Sun et al., 2014) and induce mucus release and bronchoconstriction in mice (Centeio et al., 2021). E_{act} was reported to increase $I_{TMEM16A}$ (and to a lesser extent $I_{TMEM16B}$) without elevating $[Ca^{2+}]_i$. In other words, although TMEM16A requires Ca^{2+} for activation, E_{act} still activated TMEM16A without Ca^{2+}, indicating that it is a direct activator of TMEM16A (Namkung et al., 2011).

However, a recent study found that E_{act} failed to produce a significant effect in bronchial epithelial

and FRT cells expressing endogenous TMEM16A (Genovese et al., 2019), which has raised doubts about the direct activation of TMEM16A by E_{act}. With this, Genovese et al. suggested that E_{act} may act in a cell type-dependent manner, such that it may not directly activate and potentiate TMEM16A but rather have an indirect effect. A previous report also found that E_{act} can directly activate the Ca^{2+}-permeable Transient Receptor Potential Vanilloid 1 (TRPV1) channel in mTRPV1-expressing HEK293T cells (Liu et al., 2016). Electrophysiological recordings showed that the E_{act}-induced current in neurones was not reversed when E_{act} was co-applied with a selective TMEM16A inhibitor, but was substantially reduced when co-applied with TRPV1 inhibitors (Liu et al., 2016). Considering these observations, Genovese and colleagues focused on the TRP superfamily of channels and found that E_{act} also acts on TRPV4 channels as E_{act}'s effect was inhibited by TRPV4 antagonists. These results question the specificity of E_{act} to TMEM16A channels and instead suggest that E_{act} may act through other Ca^{2+}-dependent mechanisms independent of TMEM16A, such as by activating a Ca^{2+}-permeable channel like TRPV1 or TRPV4 to promote Ca^{2+}-influx through the plasma membrane.

Yet another recent study showed that the application of E_{act} or a TRPV4 activator failed to elicit $I_{TMEM16A}$ in different cell-types expressing endogenous TMEM16A and TRPV4 channels (Centeio et al., 2020). Interestingly, quantitative Ca^{2+}-measurement revealed that E_{act} only induced a marginal increase in $[Ca^{2+}]_i$ in HEK293 cells. Co-application of the CaCC inhibitor NFA with E_{act} produced the same small increase in $[Ca^{2+}]_i$ as E_{act} alone, indicating that the above effect is TMEM16A-independent. Therefore, the authors speculated that this marginal increase in $[Ca^{2+}]_i$ was insufficient to activate TRPV4 channels, which is why E_{act} failed to indirectly activate

endogenous TMEM16A channels. However, it was observed that the application of E_{act} and other putative TMEM16A modulators potently activated overexpressed TMEM16A channels in HEK293 cells at basal $[Ca^{2+}]_i$. This observation is conflictive, as it supports that E_{act} can directly activate TMEM16A without involving an increase in $[Ca^{2+}]_i$ in HEK293 cells, contradicting the findings presented by Genovese et al in 2019. If endogenous TRPV4 channels are indeed readily expressed in HEK293 cells as shown in Centeio et al., 2020, we may expect that the E_{act}-induced $[Ca^{2+}]_i$ increase can also affect the Ca^{2+}-sensitive SK2 channels overexpressed in HEK293 cells assuming that E_{act} acts indirectly by activating TRPV4 channels. The results of the present study show that E_{act} in high concentration does not have any significant effect on SK channels, indicating that E_{act} does not directly nor indirectly activate SK2 channels in HEK293 cells. How E_{act} may act on TMEM16A remains conflictive and requires further studies. Nonetheless, as long as the specificity of E_{act} for CaCCs rests uncertain, caution should be taken when interpreting the physiological effects produced by using E_{act} as a TMEM16A-targeted activator.

Most of the TMEM16A and TMEM16B modulators lack potency and/or selectivity. Ani9 was one of the first small molecules to be described as a potent inhibitor that is highly selective for TMEM16A over TMEM16B (Seo et al., 2016). This can be seen from the results presented in this study provided by Dr Boccaccio, in which whole-cell patch-clamp recordings on HEK293A cells expressing hTMEM16A showed that Ani9 (30 μM) caused almost complete inhibition of TMEM16A (IC_{50} = 3 μM) yet had a negligible effect on TMEM16B with the same concentrations (Fig. 5 and 6). This high specificity should permit Ani9 to be used to confirm the molecular identity of chloride currents in specific tissues, as mentioned above. For instance, the application of the CaCC

inhibitor CaCCinh-A01, which shows similar potency for both TMEM16A and TMEM16B, produced stronger inhibition of CaCC whole-cell currents in cone photoreceptors compared to the same concentration of the TMEM16A-selective Ani9 (Wen and Thoreson, 2019). This finding confirms the conclusions from previous studies which suggested that TMEM16B is the predominant CaCC subtype present in cones (Stöhr et al., 2009).

Similarly, the specificity of other TMEM16A and TMEM16B inhibitors is also largely unknown. Some studies have found that CaCC blockers NPPB and tamoxifen (Burow et al., 2015), as well as the small molecules T16Ainh-01 and MONNA (Seo et al., 2016), can strongly inhibit VRACs. Experiments with yellow fluorescent protein (YFP)-quenching, an assay that indicate CaCC activity by measuring the kinetics of iodine-influx in CaCC-expressing cells transfected with YFP-based halide sensor (Namkung et al., 2010); showed that high concentration Ani9 had little effect on VRAC activity in cells expressing endogenous Volume-Regulated Anion Channels (VRAC), or on other channels including cystic fibrosis transmembrane conductance regulators (CFTR) and epithelial Na^+ channels (ENaC) (Seo et al., 2016). Moreover, other studies also showed that other TMEM16A-inhibitors CaCCinhA-01, NFA (Cabrita et al., 2017), niclosamide and benzbromarone (Cabrita et al., 2019) can block ATP-induced Ca^{2+} increase; suggesting that their inhibition mechanism may be TMEM16A-independent acting through Ca^{2+}-regulating proteins. Even the specificity of Ani9 is also questioned: patch-clamp tail-current recordings showed that Ani9 changed the gating properties of TMEM16F channels in HEK293 cells, suggesting that Ani9 may have some effect on other TMEM16 paralogues (Centeio et al., 2020). As TMEM16A and TMEM16F have been found expressed in the same tissue and speculated to contribute to the

same physiological processes such as cell migration (Jacobsen et al., 2013), further specificity testing experiments of Ani9 on TMEM16F - as well as on other ion channels in different cell types - is desirable.

Due to the lack of selective TMEM16A or TMEM16B inhibitors, many studies have use gene silencing approaches to investigate the physiological role of TMEM16A and TMEM16B in different tissues, such as using TMEM16A/ANO1 or TMEM16B/ANO2 knockout (KO) or knockdown (KD) animals. For instance, mutant TMEM16A-KO ($TMEM16A^{-/-}$) or TMEM16B-KO ($TMEM16B^{-/-}$) mice can be generated using the Cre-LoxP system by inactivating the target gene site-specifically within the expression domain of the protein Cre-recombinase (Amjad et al., 2015, Billig et al., 2011). Recently, $TMEM16A^{-/-}$ mice were generated using the CRISPR-Cas9 technology (Vyas et al., 2022). KD-animals can be generated by using a small interfering RNA (siRNA) or small hairpin RNA (shRNA) of the target gene. The siRNA or shRNA can then be injected into the animal through a vector such as a lentiviral transfer vector or an adeno-associated virus (AAV) to knock-down TMEM16A or TMEM16B (Ha et al., 2016). However, these approaches have limitations. Firstly, these gene silencing procedures are time-consuming and complex - mutant mice need to be grown for several weeks for them to be mature. Moreover, siRNA-KD is mostly limited to cell lines or primary cell cultures in vitro (Bradley et al., 2014). Furthermore, it is unclear whether loss of activity during development will mask the role of the gene in the adult state in non-conditional knockouts. Consequently, pharmacological approaches remain to be the gold-standard for assessing the functional properties of CaCCs as they are easy to manipulate and more accessible. Therefore, full characterisation of the effect of TMEM16A and TMEM16B inhibitors and activators

on CaCC-currents is essential. Importantly, modulators selective to TMEM16B remain to be characterised.

Most of the work concerning CaCC has been explored in non-neuronal tissues. However, CaCC currents have also been observed in the CNS, including in the hippocampus (Huang et al., 2012b), cerebellum (Zhang et al., 2017, Auer et al., 2021) and thalamocortical (TC) regions (Ha et al., 2016). Different techniques including RT-PCR and immunohistochemical staining, combined with pharmacological and electrophysiological techniques on ANO2-KO or shANO2-KD mice, were used to show that TMEM16B/ANO2 is the main player responsible for the CaCC-current observed in these tissues. K_{Ca}-subtypes SK and BK channels are also widely expressed in these locations and are known to play important roles in the modulation of neuronal firing. Particularly, SK channels are known to mediate Ca^{2+}-activated mAHP currents associated with spike frequency adaptation (Pedarzani et al., 2005). However, the channels involved in activating mAHP currents in TC neurones was unclear. Because CaCCs have been reported to coexist with BK and SK channels in the inferior olivary neurones (Zhang et al., 2017), they are likely to also be co-expressed in other neuronal tissues mentioned previously. As these channels share the property of high $[Ca^{2+}]_i$ sensitivity, it is possible that K_{Ca} and ANO2 work together to regulate signal encoding in central neurones. Along this line, Ha and colleagues found that TMEM16B/ANO2 is critically involved in spike frequency adaptation and may be activated in parallel with SK channels to prevent excessive spike generation in TC neurones. Indeed, the magnitude of mAHP currents was significantly reduced and the spike frequency adaptation was almost completely eliminated in AAV-shANO2-infected TC neurones (Ha et al., 2016).

So far only a handful of studies have shown the potential mechanism of interplay between K_{Ca} and CaCC in neurones (Zhang et al., 2017, Ha et al., 2016) and their roles in neuronal signalling. How specifically these channels contribute to spike frequency adaptation and other activity-dependent modulation, and how they act differently in different neuronal tissues, remains to be elucidated. The negligible effect of TMEM16A and TMEM16B modulators Ani9 and E_{act} on SK2 channels observed in the present study hints at their potential use as pharmacological tools for dissecting the functional roles of TMEM16A and TMEM16B in future research. In the meantime, however, the specificity of Ani9 and E_{act} on IK, BK and other Ca^{2+}-sensitive channels still needs to be verified. Likewise, the specificity of other CaCC pharmacological tools needs to be tested on K_{Ca} subtypes; and their effect in functional studies needs to be carefully interpreted.

Acknowledgments

I thank my supervisor, Dr Martin Stocker, for his helpful comments and thorough guidance throughout this project; to Prof. Paola Pedarzani, for her supervision of the patch-clamp experiments, and her advice with figures and discussion; to Aoife Cosgrave for her support with technical problems; and to Elliot Pratt and Julia Siembiga for proofreading the manuscript. Lastly, I also acknowledge Dr Anna Boccaccio for kindly providing the unpublished TMEM16A and TMEM16B data of Ani9 experiments.

References

1. ADELMAN, J. P. 2016. SK channels and calmodulin. *Channels (Austin),* 10**,** 1-6.
2. ADOMAVICIENE, A., SMITH, K. J., GARNETT, H. & TAMMARO, P. 2013. Putative pore-loops of TMEM16/anoctamin channels affect channel density in cell membranes. *The Journal of Physiology,* 591**,** 3487-3505.
3. AMJAD, A., HERNANDEZ-CLAVIJO, A., PIFFERI, S., MAURYA, D. K., BOCCACCIO, A., FRANZOT, J., ROCK, J. & MENINI, A. 2015. Conditional knockout of TMEM16A/anoctamin1 abolishes the calcium-activated chloride current in mouse vomeronasal sensory neurons. *J Gen Physiol,* 145**,** 285-301.
4. AUER, F., FRANCO TAVERAS, E., KLEIN, U., KESENHEIMER, C., FLEISCHHAUER, D., MÖHRLEN, F. & FRINGS, S. 2021. Anoctamin 2-chloride channels reduce simple spike activity and mediate inhibition at elevated calcium concentration in cerebellar Purkinje cells. *PLoS One,* 16**,** e0247801.
5. BERG, J., YANG, H. & JAN, L. Y. 2012. Ca2+-activated Cl- channels at a glance. *Journal of cell science,* 125**,** 1367-1371.
6. BILLIG, G. M., PÁL, B., FIDZINSKI, P. & JENTSCH, T. J. 2011. Ca2+-activated Cl− currents are dispensable for olfaction. *Nature Neuroscience,* 14**,** 763-769.
7. BOCCACCIO, A., DI ZANNI, E., GRADOGNA, A. & SCHOLZ-STARKE, J. 2019. Lifting the veils on TMEM16E function. *Channels,* 13**,** 33-35.
8. BRADLEY, E., FEDIGAN, S., WEBB, T., HOLLYWOOD, M. A., THORNBURY, K. D., MCHALE, N. G. & SERGEANT, G. P. 2014. Pharmacological characterization of TMEM16A currents.

Channels (Austin, Tex.), 8**,** 308-320.

9. BUROW, P., KLAPPERSTÜCK, M. & MARKWARDT, F. 2015. Activation of ATP secretion via volume-regulated anion channels by sphingosine-1-phosphate in RAW macrophages. *Pflugers Arch,* 467**,** 1215-26.
10. CABRITA, I., BENEDETTO, R., FONSECA, A., WANITCHAKOOL, P., SIRIANANT, L., SKRYABIN, B. V., SCHENK, L. K., PAVENSTÄDT, H., SCHREIBER, R. & KUNZELMANN, K. 2017. Differential effects of anoctamins on intracellular calcium signals. *Faseb j,* 31**,** 2123-2134.
11. CABRITA, I., BENEDETTO, R., SCHREIBER, R. & KUNZELMANN, K. 2019. Niclosamide repurposed for the treatment of inflammatory airway disease. *JCI Insight,* 4.
12. CAPUTO, A., CACI, E., FERRERA, L., PEDEMONTE, N., BARSANTI, C., SONDO, E., PFEFFER, U., RAVAZZOLO, R., ZEGARRA-MORAN, O. & GALIETTA, L. J. 2008. TMEM16A, a membrane protein associated with calcium-dependent chloride channel activity. *Science,* 322**,** 590-4.
13. CENTEIO, R., CABRITA, I., BENEDETTO, R., TALBI, K., OUSINGSAWAT, J., SCHREIBER, R., SULLIVAN, J. K. & KUNZELMANN, K. 2020. Pharmacological Inhibition and Activation of the Ca(2+) Activated Cl(-) Channel TMEM16A. *International journal of molecular sciences,* 21**,** 2557.
14. CENTEIO, R., OUSINGSAWAT, J., CABRITA, I., SCHREIBER, R., TALBI, K., BENEDETTO, R., DOUŠOVÁ, T., VERBEKEN, E. K., DE BOECK, K., COHEN, I. & KUNZELMANN, K. 2021. Mucus Release and Airway Constriction by TMEM16A May Worsen Pathology in Inflammatory Lung Disease. *International journal of molecular sciences,* 22**,** 7852.

15. CROSS, N. L. 1981. Initiation of the activation potential by an increase in intracellular calcium in eggs of the frog, Rana pipiens. *Developmental Biology,* 85**,** 380-384.
16. DANG, S., FENG, S., TIEN, J., PETERS, C. J., BULKLEY, D., LOLICATO, M., ZHAO, J., ZUBERBÜHLER, K., YE, W., QI, L., CHEN, T., CRAIK, C. S., JAN, Y. N., MINOR, D. L., JR., CHENG, Y. & JAN, L. Y. 2017. Cryo-EM structures of the TMEM16A calcium-activated chloride channel. *Nature,* 552**,** 426-429.
17. FALLAH, G., RÖMER, T., DETRO-DASSEN, S., BRAAM, U., MARKWARDT, F. & SCHMALZING, G. 2011. TMEM16A(a)/anoctamin-1 shares a homodimeric architecture with CLC chloride channels. *Mol Cell Proteomics,* 10**,** M110.004697.
18. GENOVESE, M., BORRELLI, A., VENTURINI, A., GUIDONE, D., CACI, E., VISCIDO, G., GAMBARDELLA, G., DI BERNARDO, D., SCUDIERI, P. & GALIETTA, L. J. V. 2019. TRPV4 and purinergic receptor signalling pathways are separately linked in airway epithelia to CFTR and TMEM16A chloride channels. *J Physiol,* 597**,** 5859-5878.
19. HA, G. E., LEE, J., KWAK, H., SONG, K., KWON, J., JUNG, S.-Y., HONG, J., CHANG, G.-E., HWANG, E. M., SHIN, H.-S., LEE, C. J. & CHEONG, E. 2016. The Ca2+-activated chloride channel anoctamin-2 mediates spike-frequency adaptation and regulates sensory transmission in thalamocortical neurons. *Nature Communications,* 7**,** 13791.
20. HARTZELL, H. C., YU, K., XIAO, Q., CHIEN, L.-T. & QU, Z. 2009. Anoctamin/TMEM16 family members are Ca2+-activated Cl− channels. *The Journal of Physiology,* 587**,** 2127-2139.
21. HIRSCHBERG, B., MAYLIE, J., ADELMAN, J. P. & MARRION, N. V. 1998. Gating of recombinant small-conductance Ca-activated K+ channels by calcium. *The Journal of general physiology,* 111**,** 565-581.

22. HUANG, F., WONG, X. & JAN, L. Y. 2012a. International Union of Basic and Clinical Pharmacology. LXXXV: Calcium-Activated Chloride Channels. *Pharmacological Reviews,* 64**,** 1-15.

23. HUANG, W. C., XIAO, S., HUANG, F., HARFE, B. D., JAN, Y. N. & JAN, L. Y. 2012b. Calcium-activated chloride channels (CaCCs) regulate action potential and synaptic response in hippocampal neurons. *Neuron,* 74**,** 179-92.

24. JACOBSEN, K. S., ZEEBERG, K., SAUTER, D. R. P., POULSEN, K. A., HOFFMANN, E. K. & SCHWAB, A. 2013. The role of TMEM16A (ANO1) and TMEM16F (ANO6) in cell migration. *Pflugers Archiv : European journal of physiology,* 465**,** 1753-1762.

25. KÖHLER, M., HIRSCHBERG, B., BOND, C. T., KINZIE, J. M., MARRION, N. V., MAYLIE, J. & ADELMAN, J. P. 1996. Small-conductance, calcium-activated potassium channels from mammalian brain. *Science,* 273**,** 1709-14.

26. KUNZELMANN, K., OUSINGSAWAT, J., CABRITA, I., DOUŠOVÁ, T., BÄHR, A., JANDA, M., SCHREIBER, R. & BENEDETTO, R. 2019. TMEM16A in Cystic Fibrosis: Activating or Inhibiting? *Frontiers in Pharmacology,* 10.

27. LAM, A. K. M. & DUTZLER, R. 2018. Calcium-dependent electrostatic control of anion access to the pore of the calcium-activated chloride channel TMEM16A. *eLife,* 7.

28. LE, S. C., JIA, Z., CHEN, J. & YANG, H. 2019a. Molecular basis of PIP(2)-dependent regulation of the Ca(2+)-activated chloride channel TMEM16A. *Nat Commun,* 10**,** 3769.

29. LE, S. C. & YANG, H. 2020. An Additional Ca2+ Binding Site Allosterically Controls TMEM16A Activation. *Cell Reports,* 33**,** 108570.

30. LE, T., JIA, Z., LE, S. C., ZHANG, Y., CHEN, J. & YANG, H. 2019b. An inner activation gate

controls TMEM16F phospholipid scrambling. *Nature Communications,* 10**,** 1846.

31. LIM, N. K., LAM, A. K. & DUTZLER, R. 2016. Independent activation of ion conduction pores in the double-barreled calcium-activated chloride channel TMEM16A. *J Gen Physiol,* 148**,** 375-392.
32. LIU, S., FENG, J., LUO, J., YANG, P., BRETT, T. J. & HU, H. 2016. Eact, a small molecule activator of TMEM16A, activates TRPV1 and elicits pain- and itch-related behaviours. *British journal of pharmacology,* 173**,** 1208-1218.
33. NAMKUNG, W., THIAGARAJAH, J. R., PHUAN, P.-W. & VERKMAN, A. S. 2010. Inhibition of Ca2+-activated Cl− channels by gallotannins as a possible molecular basis for health benefits of red wine and green tea. *The FASEB Journal,* 24**,** 4178-4186.
34. NAMKUNG, W., YAO, Z., FINKBEINER, W. E. & VERKMAN, A. S. 2011. Small-molecule activators of TMEM16A, a calcium-activated chloride channel, stimulate epithelial chloride secretion and intestinal contraction. *Faseb j,* 25**,** 4048-62.
35. NOLTING, A., FERRARO, T., D'HOEDT, D. & STOCKER, M. 2007. An Amino Acid Outside the Pore Region Influences Apamin Sensitivity in Small Conductance Ca2+-activated K+ Channels*. *Journal of Biological Chemistry,* 282**,** 3478-3486.
36. PAULINO, C., KALIENKOVA, V., LAM, A. K. M., NELDNER, Y. & DUTZLER, R. 2017a. Activation mechanism of the calcium-activated chloride channel TMEM16A revealed by cryo-EM. *Nature,* 552**,** 421-425.
37. PAULINO, C., NELDNER, Y., LAM, A. K. M., KALIENKOVA, V., BRUNNER, J. D., SCHENCK, S. & DUTZLER, R. 2017b. Structural basis for anion conduction in the calcium-activated chloride channel TMEM16A. *eLife,* 6**,** e26232.

38. PEDARZANI, P., MCCUTCHEON, J. E., ROGGE, G., JENSEN, B. S., CHRISTOPHERSEN, P., HOUGAARD, C., STRØBAEK, D. & STOCKER, M. 2005. Specific enhancement of SK channel activity selectively potentiates the afterhyperpolarizing current I(AHP) and modulates the firing properties of hippocampal pyramidal neurons. *J Biol Chem,* 280**,** 41404-11.
39. PEDARZANI, P. & STOCKER, M. 2008. Molecular and cellular basis of small--and intermediate-conductance, calcium-activated potassium channel function in the brain. *Cell Mol Life Sci,* 65**,** 3196-217.
40. PETERS, C. J., GILCHRIST, J. M., TIEN, J., BETHEL, N. P., QI, L., CHEN, T., WANG, L., JAN, Y. N., GRABE, M. & JAN, L. Y. 2018. The Sixth Transmembrane Segment Is a Major Gating Component of the TMEM16A Calcium-Activated Chloride Channel. *Neuron,* 97**,** 1063-1077.e4.
41. PIFFERI, S., DIBATTISTA, M. & MENINI, A. 2009. TMEM16B induces chloride currents activated by calcium in mammalian cells. *Pflugers Arch,* 458**,** 1023-38.
42. SCHROEDER, B. C., CHENG, T., JAN, Y. N. & JAN, L. Y. 2008. Expression cloning of TMEM16A as a calcium-activated chloride channel subunit. *Cell,* 134**,** 1019-29.
43. SCUDIERI, P., SONDO, E., FERRERA, L. & GALIETTA, L. J. V. 2012. The anoctamin family: TMEM16A and TMEM16B as calcium-activated chloride channels. *Experimental Physiology,* 97**,** 177-183.
44. SEO, Y., LEE, H. K., PARK, J., JEON, D.-K., JO, S., JO, M. & NAMKUNG, W. 2016. Ani9, A Novel Potent Small-Molecule ANO1 Inhibitor with Negligible Effect on ANO2. *PloS one,* 11**,** e0155771-e0155771.
45. SHERIDAN, J. T., WORTHINGTON, E. N., YU, K., GABRIEL, S. E., HARTZELL, H. C. & TARRAN, R. 2011. Characterization of the Oligomeric Structure of the Ca2+-activated Cl−

Channel Ano1/TMEM16A*. *Journal of Biological Chemistry,* 286**,** 1381-1388.

46. SOH, H. & PARK, C. S. 2001. Inwardly rectifying current-voltage relationship of small-conductance Ca2+-activated K+ channels rendered by intracellular divalent cation blockade. *Biophys J,* 80**,** 2207-15.
47. STOCKER, M. & PEDARZANI, P. 2000. Differential distribution of three Ca(2+)-activated K(+) channel subunits, SK1, SK2, and SK3, in the adult rat central nervous system. *Mol Cell Neurosci,* 15**,** 476-93.
48. STÖHR, H., HEISIG, J. B., BENZ, P. M., SCHÖBERL, S., MILENKOVIC, V. M., STRAUSS, O., AARTSEN, W. M., WIJNHOLDS, J., WEBER, B. H. & SCHULZ, H. L. 2009. TMEM16B, a novel protein with calcium-dependent chloride channel activity, associates with a presynaptic protein complex in photoreceptor terminals. *J Neurosci,* 29**,** 6809-18.
49. SUN, M., SUI, Y., LI, L., SU, W., HAO, F., ZHU, Q., DI, W., GAO, H. & MA, T. 2014. Anoctamin 1 calcium-activated chloride channel downregulates estrogen production in mouse ovarian granulosa cells. *Endocrinology,* 155**,** 2787-96.
50. SUZUKI, J., FUJII, T., IMAO, T., ISHIHARA, K., KUBA, H. & NAGATA, S. 2013. Calcium-dependent Phospholipid Scramblase Activity of TMEM16 Protein Family Members *. *Journal of Biological Chemistry,* 288**,** 13305-13316.
51. TERASHIMA, H., PICOLLO, A. & ACCARDI, A. 2013. Purified TMEM16A is sufficient to form Ca2+-activated Cl- channels. *Proc Natl Acad Sci U S A,* 110**,** 19354-9.
52. TIEN, J., PETERS, C. J., WONG, X. M., CHENG, T., JAN, Y. N., JAN, L. Y. & YANG, H. 2014. A comprehensive search for calcium binding sites critical for TMEM16A calcium-activated chloride channel activity. *eLife,* 3**,** e02772.

53. VYAS, A., GOMEZ-CASAL, R., CRUZ-RANGEL, S., VILLANUEVA, H., SIKORA, A. G., RAJAGOPALAN, P., BASU, D., PACHECO, J., HAMMOND, G. R. V., KISELYOV, K. & DUVVURI, U. 2022. Lysosomal inhibition sensitizes TMEM16A-expressing cancer cells to chemotherapy. *Proceedings of the National Academy of Sciences,* 119**,** e2100670119.

54. WEN, X. & THORESON, W. B. 2019. Contributions of glutamate transporters and Ca(2+)-activated Cl(-) currents to feedback from horizontal cells to cone photoreceptors. *Experimental eye research,* 189**,** 107847-107847.

55. XIAO, Q., YU, K., PEREZ-CORNEJO, P., CUI, Y., ARREOLA, J. & HARTZELL, H. C. 2011. Voltage- and calcium-dependent gating of TMEM16A/Ano1 chloride channels are physically coupled by the first intracellular loop. *Proceedings of the National Academy of Sciences,* 108**,** 8891-8896.

56. YANG, Y. D., CHO, H., KOO, J. Y., TAK, M. H., CHO, Y., SHIM, W. S., PARK, S. P., LEE, J., LEE, B., KIM, B. M., RAOUF, R., SHIN, Y. K. & OH, U. 2008. TMEM16A confers receptor-activated calcium-dependent chloride conductance. *Nature,* 455**,** 1210-5.

57. YU, K., WHITLOCK, J. M., LEE, K., ORTLUND, E. A., YUAN CUI, Y. & HARTZELL, H. C. 2015. Identification of a lipid scrambling domain in ANO6/TMEM16F. *eLife,* 4**,** e06901.

58. YU, K., ZHU, J., QU, Z., CUI, Y.-Y. & HARTZELL, H. C. 2014. Activation of the Ano1 (TMEM16A) chloride channel by calcium is not mediated by calmodulin. *The Journal of general physiology,* 143**,** 253-267.

59. ZHANG, Y., ZHANG, Z., XIAO, S., TIEN, J., LE, S., LE, T., JAN, L. Y. & YANG, H. 2017. Inferior Olivary TMEM16B Mediates Cerebellar Motor Learning. *Neuron,* 95**,** 1103-1111.e4.